

Organ-Level Radiation Doses from CT Scans for 10,000 Chinese Subjects Undergoing Physical Examinations: The Feasibility of AI-Based Multi-organ CT Image Segmentation and Near Real-time Monte Carlo Dose Computing

Zirui Ye¹, Bei Yao², Haoran Zheng², Li Tao¹, Ripeng Wang¹, Yang Lu³, Yankui Chang¹, Xi Pei³, Zhi Chen¹,
Xie George Xu^{1,2,4*}

¹ School of Nuclear Science and Technology, University of Science and Technology of China, Hefei 230026, China

² Department of Radiation Oncology, The First Affiliated Hospital, University of Science and Technology of China, Hefei 230001, China

³ Anhui Wisdom Technology Co., Ltd., Hefei 238000, China

⁴ Deep Space Exploration Laboratory, University of Science and Technology of China, Hefei 230026, China.

Corresponding author:

Professor Xie George Xu, Ph.D. FAIMBE, FAAPM, FHPS, FANS

University of Science and Technology of China

Huangshan Road 443, Hefei 230026, Anhui, China

Email: xgxu@ustc.edu.cn

Abstract

Considering the increasing trend of physical examinations in China, the escalating frequency of Computed Tomography (CT) scans has amplified concerns regarding population radiation exposure and its consequent risks. The challenges mainly manifest in two aspects: one is the rapid construction of patient-specific human phantoms, and the other is the fast Monte Carlo (MC) simulation of radiation dose. Hence, this study aims to demonstrate a near real-time MC patient-specific organ dose computation method, for the first time, involving automatic segmentation across a large dataset of 11,482 subjects undergoing chest CT scans. We developed a preliminary software platform, integrating the automatic segmentation software DeepViewer and the GPU-accelerated MC engine ARCHER-CT. Comparisons with traditional dosimetry methods revealed up to 100% discrepancies for a few subjects in organ-level dose, underscoring the patient-specific method's superior accuracy. This study paves the way for more accurate radiation risk assessment, crucial in the era of patient-specific radiation dosimetry.

Computed Tomography (CT) scanning represents the principal contributor to the global average annual effective dose per individual from non-therapeutic medical radiation sources^{1,2}. In China, the checklist for physical examination has increasingly included an item called X-ray CT scan – a medical imaging procedure that can detect tiny lung lesions but is known to pose a small risk of radiation exposure to the employee whose examination fee is possibly paid by his or her employer, as stipulated by the labor law. Although the number of CT scans per capita in China today is still relatively low in comparison with many developed countries, the total number of medically exposed Chinese individuals (to CT and other X-ray related procedures) is rising at alarming rate. In Shanghai, China, the annual frequency of CT examinations in 2016 reached 304 per thousand people, which is 2.74 times

that of 2007³. The most recent epidemiological analysis indicates that in a cohort of 10,000 children undergoing CT scans with an average exposure of 8 mGy, approximately 1 to 2 individuals may develop hematological malignancies attributable to this radiation, within the following 12 years⁴. Worldwide, there has been a strong desire to estimate and to manage radiation risk from CT examinations. One of the challenges in understanding the severity of CT related risk is the lack of computational tools to track organ-level radiation doses. After all, assessment of radiation risk should be ideally based on radiation dose to the exposed organs or tissues, according to the BEIR VII report⁵. Consequently, the precision in estimating organ-level doses is essential for the reliability of radiation risk assessments.

The challenges in estimating patient-specific organ-level dose mainly manifest in two aspects: one is the rapid construction of patient-specific computational human phantoms, and the other is the fast and accurate calculation of radiation dose. However, to manually delineate patient-specific radiosensitive organs or tissues from CT images of a large number of subjects can be laborious. Furthermore, the “gold standard” dose calculations rely on computational methods known as Monte Carlo (MC) simulations that are computationally expensive due to the statistical nature of the method⁶. These difficulties are acute when considering the application of such methodologies in large-scale clinical settings. Thus, developing a tool for swiftly and accurately calculating patient-specific organ-level doses during CT scans is important.

There are two mature methods for calculating organ-level doses in CT scans: dosimetry parameters and population-averaged phantom simulation. However, these methods are not accurate enough for individual subjects. On the one hand, conventional dosimetry metrics like volume CT Dose Index (CTDI_{vol}), Dose-Length Product (DLP), and Size-Specific Dose Estimates (SSDE), often paired with respective conversion factors, are applied to estimate organ-level and effective doses, but their inability to account for the distinct anatomical structures of individual subjects can lead to inaccuracies in representing the true organ doses received^{7–11}. On the other hand, digital human phantoms have evolved into Boundary Representation (BREP) phantoms, which are the third generation of computational phantoms¹². These phantoms typically categorize populations by gender, Body Mass Index (BMI), and age groups¹³. Based on the population-averaged phantoms, validated CT scanner models and dose database of MC simulations, several teams have developed CT subject radiation dose estimation software, such as WAZA-ARI¹⁴, VirtualDose¹⁵, NCICT¹⁶, and MIRDct¹⁷. Software solutions like VirtualDose offer improvements in anatomical diversity compared to the International Commission on Radiological Protection (ICRP) reference phantoms¹⁸. However, these solutions rely on the best-matching pre-built phantom from their libraries, rather than generating a patient-specific phantom. Additionally, aligning the scan range for a population-averaged phantom with that of the actual subject remains a challenge¹⁹.

In recent years, automatic organ segmentation based on Artificial Intelligence (AI)²⁰, and Graphics Processing Unit (GPU) accelerated Monte Carlo methods^{21,22}, have shown promise in the field of radiation dosimetry. Therefore, a few studies have explored the methods combining these two technologies with validated CT scanner models^{23,24}, so as to gauge the feasibility of providing patient-specific organ-level dose estimates for CT scan subjects. However, these related studies have not incorporated data from large sample sizes exceeding 10,000 subjects. Consequently, they fall short of fully substantiating the speed, accuracy, and superiority of real-time patient-specific dosimetry over traditional population-averaged phantom methodologies.

Thus, this study aims to demonstrate a method for the near real-time estimation of patient-specific organ-level radiation doses during CT scans, scalable for hospital applications. We utilized a commercial software, DeepViewer^{24–26}, integrated with a convolutional neural network (CNN)-based CT image automatic organ segmentation method, to construct patient-specific phantoms for subjects. Besides, we employed the GPU-accelerated MC dose calculation software, ARCHER-CT²¹, for simulation of X-ray transport and dosimetry, aligned with a validated CT scanner model. As illustrated in Figure 1, a preliminary CT dose calculation and analysis software platform based on the dosimetry engine was developed, and it was tested on a large dataset comprising

11,482 subjects from the Health Center of the First Affiliated Hospital of the University of Science and Technology of China.

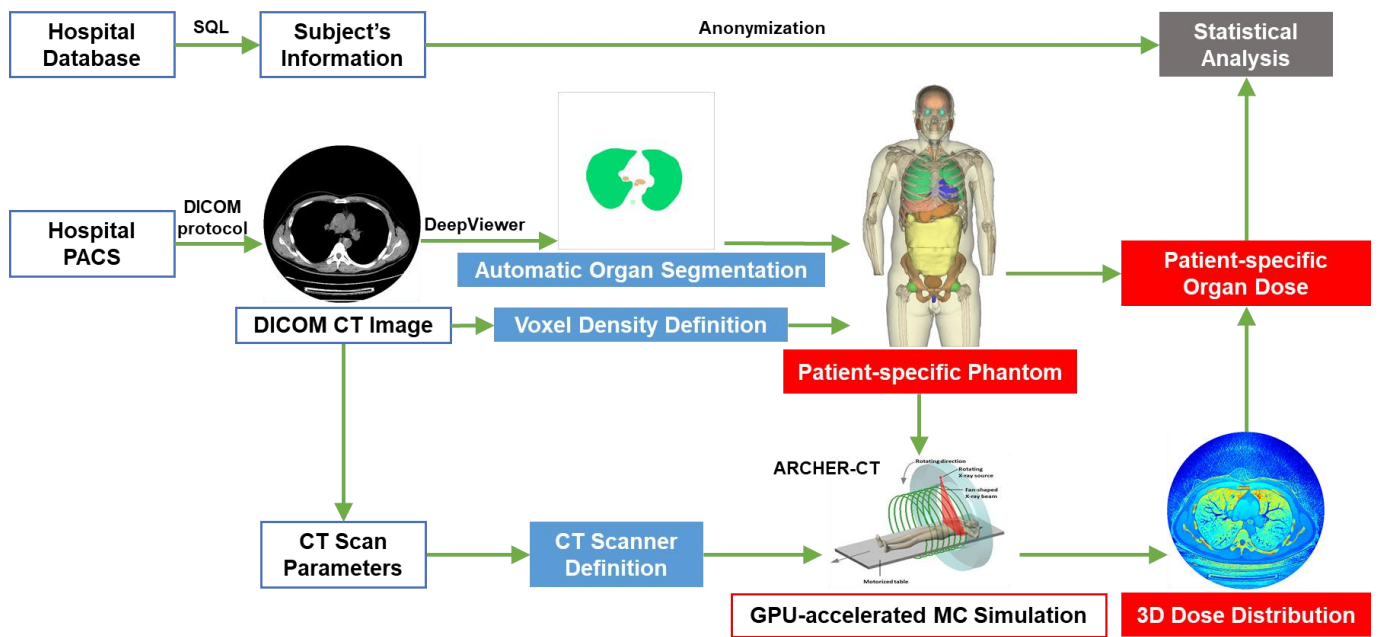


Figure 1. The flow chart of a preliminary CT dose computation and analysis software platform based on the dosimetry engine. After the subject's CT images were automatically segmented and the corresponding patient-specific phantom was constructed, a near real-time dose simulation on the phantom using a chest scan protocol similar to that used in clinical image acquisition was performed. Based on the organ doses obtained and subject's information extracted, statistical analysis could be finished.

For each CT scan subject, the average simulation time for ARCHER-CT was 4.8 seconds, and the mean time for DeepViewer's preprocessing and automatic segmentation was approximately 173 seconds. Figure 2 presents a visualization example of a patient-specific phantom constructed from a subject's chest CT data using DeepViewer, and the dose distribution simulated by ARCHER-CT.

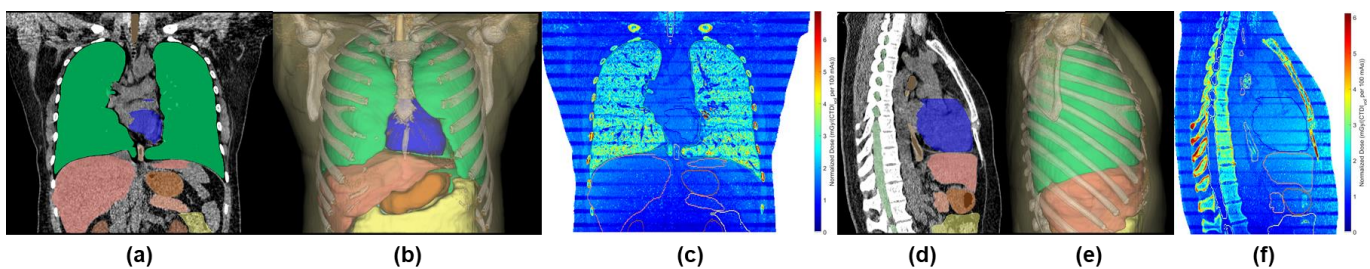


Figure 2. A visualization example of a patient-specific phantom constructed from a subject's chest CT data using DeepViewer. (a)(c) The 2D views of the coronal and sagittal planes of the CT image and automatic segmentation masks. (b)(d) The 3D views of the anterior and lateral perspectives of the geometric phantom. (c)(f) The 2D views of the anterior and lateral perspectives of the $CTDI_{vol}$ normalized dose distribution and automatic segmentation masks.

Results

Comparison of the proposed patient-specific method and the ICRP reference phantom method

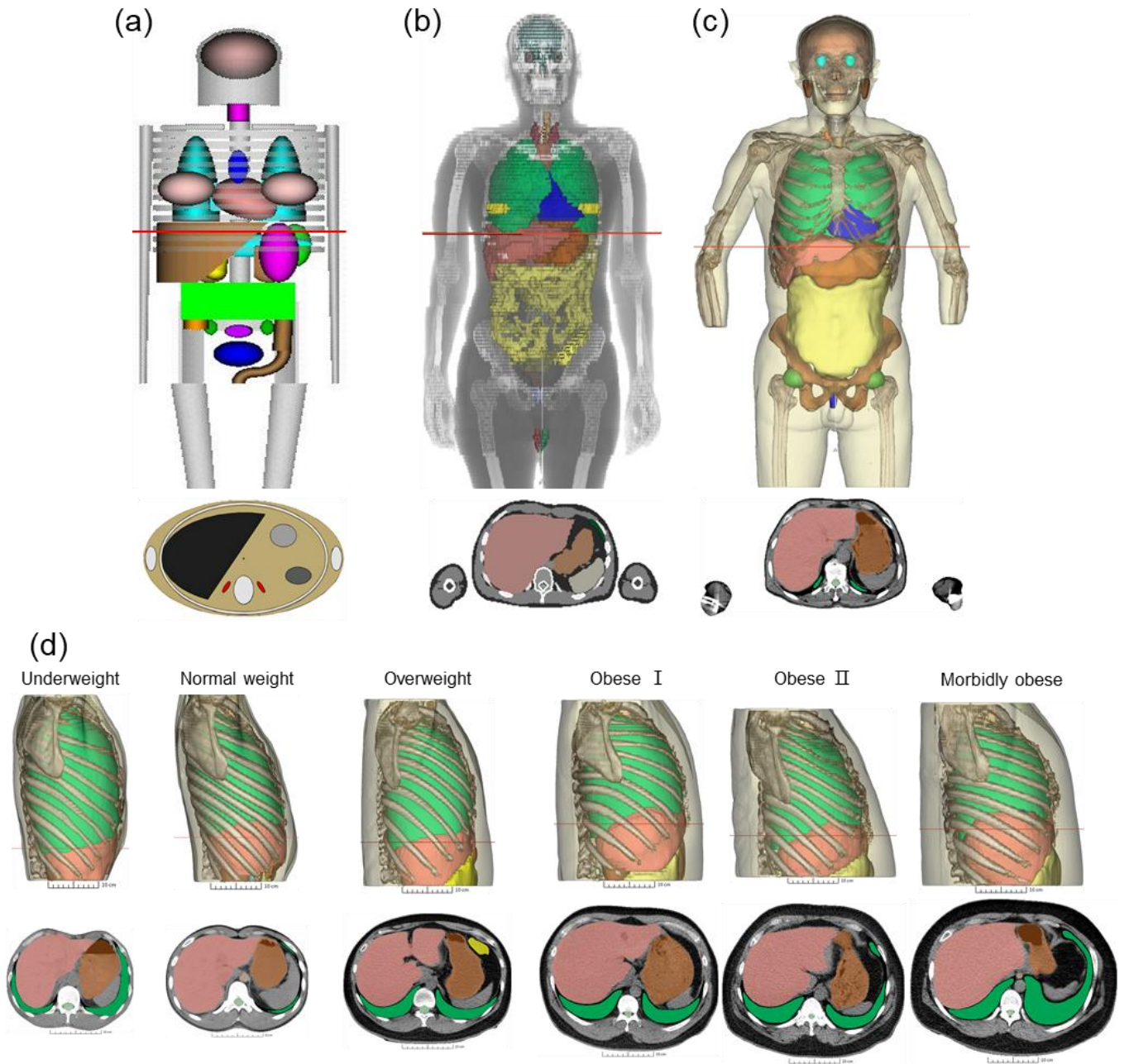


Figure 3. Comparative visualization of three generations of computational human phantoms, each including a 3D view from an anterior perspective, and a cross-sectional view at the height indicated by a red line. (a) A stylized phantom. (b) The ICRP adult male reference voxelized phantom¹⁸. (c) A patient-specific phantom for a normal-weight male subject, constructed with an AI-driven multi-organ CT image segmentation method. (d) Patient-specific male phantoms at six different BMI categories defined by the World Health Organization globally²⁷, from underweight to morbidly obese, illustrating the variations in organ shape, size and spatial relationships.

Figure 3 illustrates the discrepancies between individual subjects and population-averaged phantoms, which manifest in variations in organ shape, size, and spatial relationships. When using the population-averaged phantom method, these inconsistencies can lead to errors in organ dose estimates. Furthermore, the anatomical differences necessitate meticulous alignment of each subject's CT scan range onto the population-averaged phantom when employing this conventional method. Thus, our study contrasted the novel patient-specific method with the established ICRP reference phantom method which is a mainstay in radiation protection dosimetry¹⁸. Constructed based on standard adult stature and mass, the ICRP adult male and female reference voxelized phantoms incorporate typical organ dimensions and placements, providing a standardized basis for radiation safety standards and risk assessment. Yet, the homogeneity in tissues and organs, coupled with "population-

averaged" human anatomy and physiological characteristics in the reference phantoms, limits their applicability in precisely assessing individualized doses.

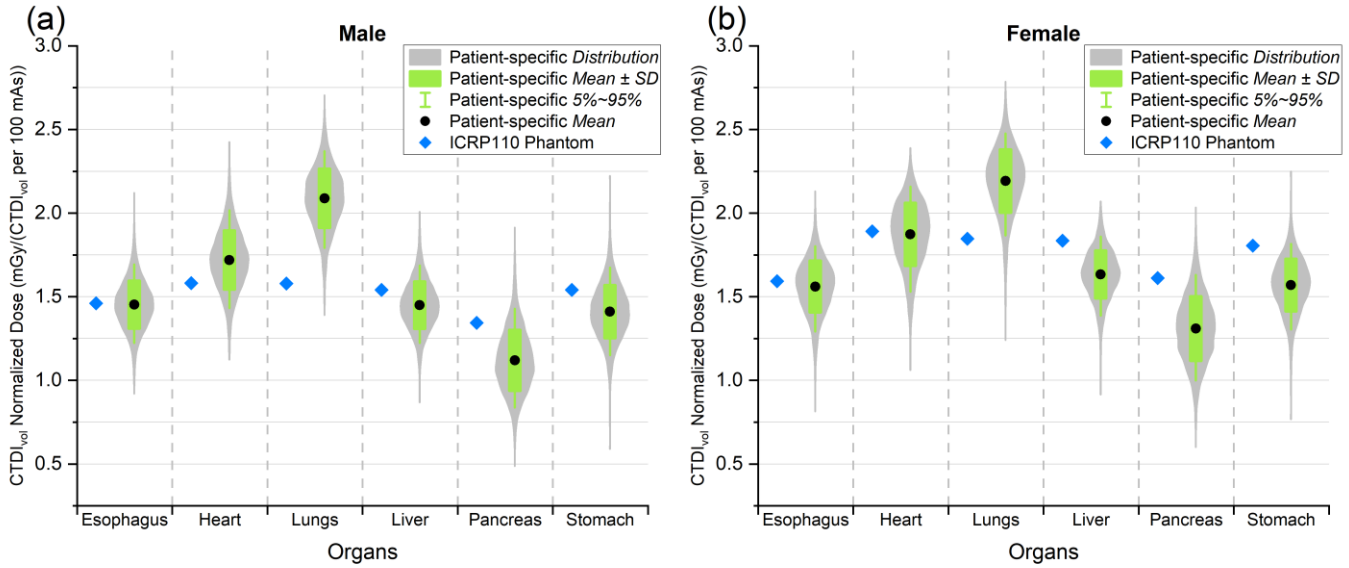


Figure 4. Comparison of the proposed patient-specific method and the ICRP reference phantom method¹⁸. The vertical axis displays the CTDI_{vol} normalized organ dose in units of mGy/(CTDI_{vol} per 100 mAs) for chest CT scan. The horizontal axis shows the 6 organs: esophagus, heart, lungs, liver, pancreas, and stomach. (a) Results for the male. (b) Results for the female.

As depicted in Figure 4, there are noticeable differences in CTDI_{vol} normalized organ doses (in mGy/(CTDI_{vol} per 100 mAs)) between the two methods. In males, the patient-specific method estimates that the organ doses for the esophagus, heart, lungs, liver, pancreas, and stomach differ by up to 45%, 53%, 71%, 44%, 64%, and 62%, respectively, in comparison to the ICRP reference phantom method. The average discrepancies for these six organs, when using the patient-specific method as opposed to the ICRP reference phantom method, are 1%, 9%, 32%, 6%, 17%, and 9%, respectively. In females, the patient-specific method estimates that the organ doses for the six organs differ by up to 49%, 44%, 51%, 50%, 63%, and 57%, respectively. The average discrepancies for these six organs are 2%, 1%, 19%, 11%, 19%, and 13%, respectively. These variances can be ascribed to the ability of the patient-specific method to accommodate individual anatomical differences.

Comparison of the proposed patient-specific method and dosimetry parameters method

To compare the accuracy between the proposed patient-specific method and dosimetry parameters method, we calculated the Water Equivalent Diameters (WED) of the 11,482 subjects. The WED, as the American Association of Physicists in Medicine (AAPM) suggested, can describe the body size of the subjects more accurately, and can be utilized for estimating the SSDE and CTDI_{vol} normalized organ dose in mGy/(CTDI_{vol} per 100 mAs)²⁸. The estimation of the SSDE is based on the conversion of the CTDI_{vol} measured using the 32 cm diameter polymethyl methacrylate (PMMA) CTDI_{vol} phantoms, to a specific subject's body size. The WED of each slice is derived from the CT values within the body region of the CT slice image, with the specific formula as follows:

$$WED = 2 \sqrt{\left(\frac{CT_{body}}{1000} + 1\right) \frac{A_{body}}{\pi}} \quad (3)$$

$$D_{from\ WED}^{normalized} = f_{size}(WED) = A \times e^{-B \times WED} \quad (4)$$

$$SSDE = f_{size}(WED) \times CTDI_{vol} \quad (5)$$

Where $\overline{CT_{body}}$ represents the average CT value of all pixels within the body region of the CT slice image, and A_{body} denotes the total area of the body region of the CT slice image. A and B are organ-specific constants.

$D_{from\ WED}^{normalized}$ is the $CTDI_{vol}$ normalized organ dose estimated from exponential fitting method. $f_{size}(WED)$ is the SSDE conversion factor. In this study, the average WED calculated across all image slices serves to characterize the overall body size of each subject. Then, we performed an exponential fitting analysis on the normalized organ dose results of the subjects and their average WED to assess the errors introduced by the method of exponential fitted dosimetry parameters, compared to the patient-specific method²⁸.

In Figure 5, we present graphs of the distribution of normalized organ doses as functions of average WED, accompanied by exponential fitting lines. The results suggest that if the exponential fitting method is used to estimate the patient-specific normalized organ dose, an average (\pm standard deviation) error of 2.8% ($\pm 2.3\%$), 2.5% ($\pm 2.1\%$), 4.4% ($\pm 3.5\%$), 4.1% ($\pm 3.1\%$), 9.5% ($\pm 7.5\%$), 5.3% ($\pm 4.4\%$) might be introduced for esophagus, heart, lungs, liver, pancreas, and stomach, respectively, for the male. And an average (\pm standard deviation) error of 3.3% ($\pm 2.5\%$), 2.8% ($\pm 2.6\%$), 4.6% ($\pm 3.8\%$), 3.9% ($\pm 3.0\%$), 10.8% ($\pm 8.4\%$), 5.9% ($\pm 4.8\%$) might be introduced for the 6 organs, respectively, for the female. Although the average difference between the results of exponential fitting method and the patient-specific method is within 10%. In the case of a few subjects' specific organ, this difference can exceed 50%. In summary, estimating the organ dose for subjects in CT scans based on the average water-equivalent diameter using the method of exponential fitted dosimetry parameters is not patient-specific accurate.

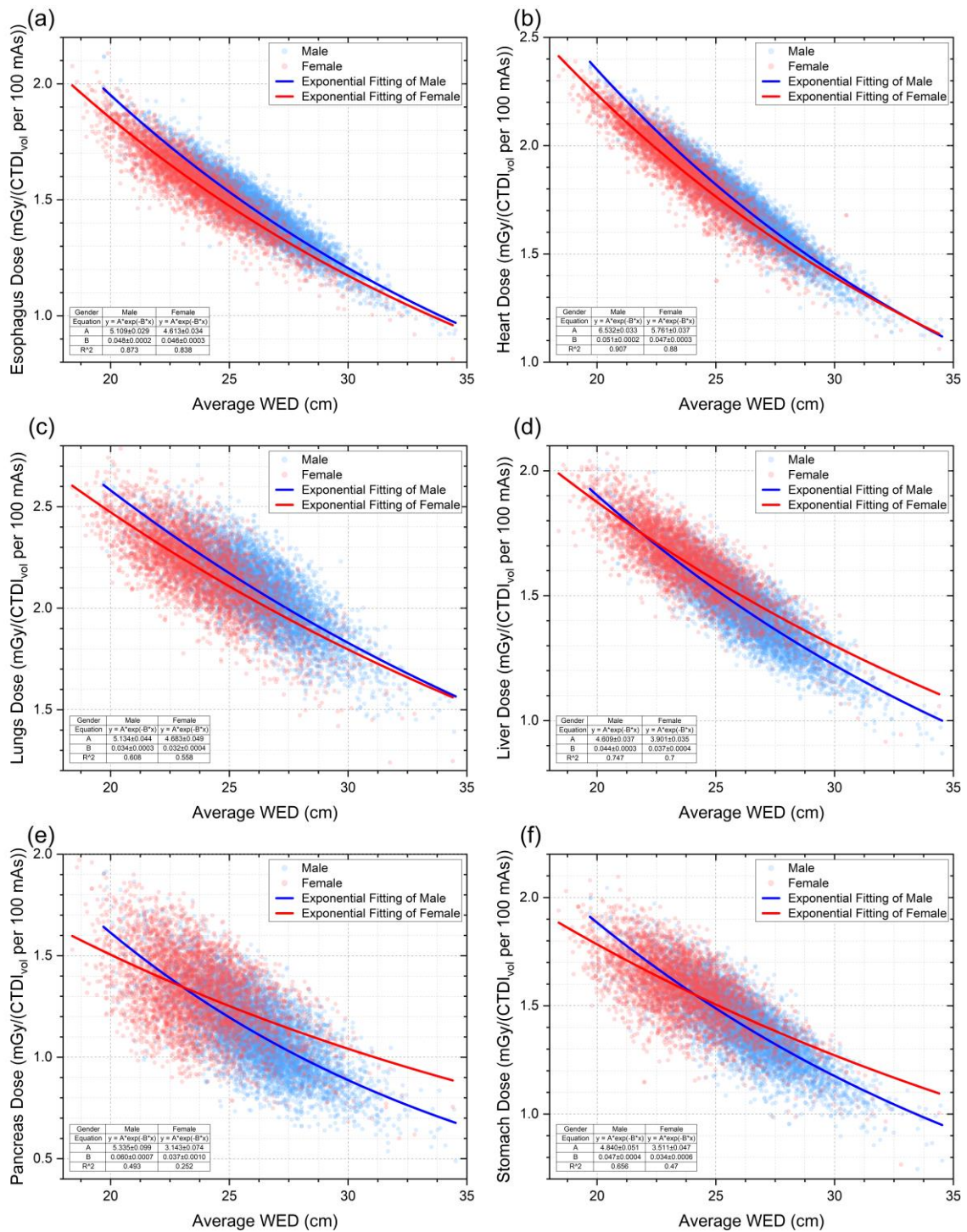


Figure 5. The graphs of the CTDI_{vol} normalized organ doses in mGy/(CTDI_{vol} per 100 mAs) during chest CT scan for the 6 organs relative to average WED, including an exponential fitting. (a) Results for esophagus. (b) Results for heart. (c) Results for lungs. (d) Results for liver. (e) Results for pancreas. (f) Results for stomach.

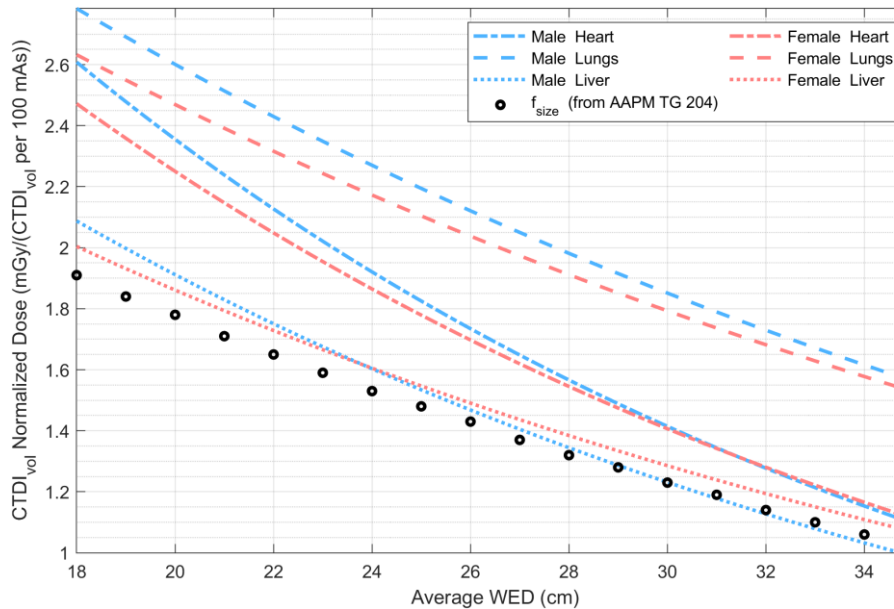


Figure 6. The exponential fitting curves of the $CTDI_{vol}$ normalized organ doses for the three organs during a chest CT scan, and data points for the SSDE conversion factor (f_{size}) provided in AAPM Report No. 204⁹, all in relation to the average WED.

As Figure 6 and Equation (5) showed, SSDE are not applicable for organ dose estimation. The proposed patient-specific method enables the accurate estimation of organ-level radiation doses, as well as advances radiation dose estimation methodologies from those based on WED and SSDE to an organ-specific level.

Discussion

In conclusion, pre-built population-averaged phantoms method and the dosimetry parameters method are not appropriate for estimating organ doses for a specific group or individual undergoing a CT scan, while the patient-specific method offers a more accurate estimation.

Overall, the DeepViewer and ARCEHR software used in this study were originally developed to meet the stringent accuracy requirements of the radiotherapy domain, namely a gamma pass rate within 5%. Therefore, their accuracy is entirely adequate for the more lenient standards of radiation protection. While the tools also have proven accuracy in previous investigations, several enhancements can be made to our proposed method before its clinical application. Specific measures include: (1) Obtaining software tools from CT scanner manufacturers to capture the start and end angles of the tube rotation and slice-specific tube current values when using Tube Current Modulation (TCM) technology, thus more accurately simulating X-ray irradiation during a helical scan. (2) Although a validated 16-detector CT scanner model was used in this study, multi-detector CT (MDCT) with more detector slices is increasingly prevalent in clinical settings. The development and validation of scanner models that are more representative of actual machines are warranted. (3) Experimentally measuring the organ doses using physical anthropomorphic phantoms under identical CT scanning conditions, then contrasting these measurements with those obtained via MC simulations, will provide an additional layer of validation. (4) Expand the simulation methods regarding over-scanning range to accurately assess the impact of scattered radiation on organ doses.

Research by Peng et al., using similar tools and methodologies, determined that the automatic segmentation tool take an average of 5 seconds per subject²⁴. In contrast, this study found the average processing times to be considerably longer at 173 seconds. Beyond hardware variations, two reasons account for this discrepancy: firstly, this study processed clinical raw imaging data directly without resampling to a reduced pixel count. Secondly, the commercial version of DeepViewer was utilized, which integrates network models for identifying CT scanning body

regions and additional preprocessing modules to ensure the robustness and accuracy of organ recognition and segmentation, thereby increasing runtime.

The patient-specific method proposed in this study can be effortlessly extended to simulate various other X-ray-based imaging techniques, such as radiography, contrast-enhanced CT scanning, tomographic synthesis, fluoroscopy, and mammography, offering a comprehensive framework for clinical dosimetry quantification. The real-time Monte Carlo techniques, based on automatic segmentation and accelerated by GPUs, can also be extended to other domains of clinical dosimetry and radiation protection, such as proton CT and nuclear medicine. Additionally, the extensive organ dose dataset generated through this methodology could serve as a resource for training deep learning networks, thereby augmenting the predictive accuracy of radiation dose estimates.

Moreover, as the concept of patient-specific effective dose evolves, precise patient-specific radiation protection dosimetry increasingly requires swift construction of full-body phantoms and real-time Monte Carlo tools²⁹. However, current CT imaging and automatic segmentation techniques can only construct phantoms corresponding to the scanned region. Hence, further development is essential in creating full-body phantoms for subjects from CT images or other data sources, integrating them with individualized radiation risk assessment methods, and ushering radiation protection dosimetry into a new phase of evolution.

This study demonstrated a near real-time Monte Carlo patient-specific organ-level dose estimation method, for the first time, involving automatic segmentation of over 10,000 subjects and conducting comprehensive statistical analysis. We verified the necessity and superiority of the proposed patient-specific method, compared to the method of exponential fitted dosimetry parameters and the conventional population-average phantom method. Our works lay the groundwork for the development of a software system that can be integrated into hospital workflows. Considering the increasing trend of physical examinations in China, the escalating frequency of CT scans has amplified concerns regarding cumulative radiation exposure and population dose burden. This study may contribute to enhancing patient-specific radiation safety, further mitigating this issue in the healthcare industry.

Methods

Data

With the approval of the Ethics Committee of the First Affiliated Hospital of the University of Science and Technology of China, this study conducted a retrospective analysis of the randomly collected clinical data from 11,482 chest CT scan subjects at the Health Center. The privacy and personal information of all subjects from whom the data were sourced were anonymized and properly protected. We obtained the subjects' age, gender, height, weight, and other information in bulk from the hospital's information system database using Structured Query Language (SQL). The image files of the chest CT scans taken during the subjects' health examinations were acquired in bulk, through the Digital Imaging and Communications in Medicine (DICOM) protocol from the hospital's Picture Archiving and Communication System (PACS) network interface. Subsequently, only images and the parameters of the CT scanner were extracted from DICOM files.

Development of a CT dose calculation and analysis software platform

In this study, we utilized the ARCHER-CT computing engine for rapid MC simulations of CT scans²¹. ARCHER-CT is implemented with a hybrid programming approach using Open Multi-Processing (OpenMP) and Compute Unified Device Architecture (CUDA), supporting CPU parallelism and multi-GPU acceleration. ARCHER-CT is capable of GPU-accelerated simulation of low-energy photon transport below 140 keV in heterogeneous media, modeling photoelectric effects, Compton scattering, and Rayleigh scattering interactions, considering the electron's binding effects in scatter simulations. As the Continuous Slowing Down Approximation (CSDA) range of the electron is generally an order of magnitude smaller than the voxel size in CT, the energy of secondary electrons is presumed to be deposited in local voxels. Besides, ARCHER-CT integrates a parameterized and experimentally

validated GE LightSpeed Pro 16 multi-detector CT (MDCT) scanner model^{15,30}. A simple schematic of the scanner modeling and a patient-specific phantom slice in a single axial scan is shown in Figure 7. On this basis, ARCHER-CT supports various CT scan protocols, including kilovoltage peak (kVp) from 80 to 140, beam collimation width from 1.25 to 20 mm, head or body bowtie filters, any pitch values, and axial or helical scanning modes. Through comparison with the general-purpose MC software Monte Carlo N-Particle (MCNP), the accuracy of ARCHER-CT has been verified in previous studies^{21,31}.

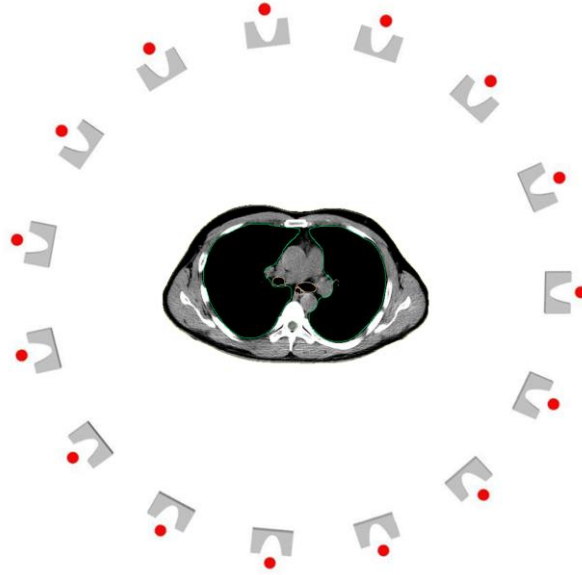


Figure 7. A simple schematic of the validated scanner modeling¹⁵ and a patient-specific phantom slice in a single axial scan. A total of 16 x-ray beam sources and bowtie filters were used.

The 3D dose distribution map, generated by the ARCHER-CT simulation normalized to each particle, was of the same size and resolution as the CT images, with the dose unit for each voxel being MeV/gram/source particle. Using this dose distribution map and the organ segmentation mask, we calculated patient-specific organ doses. To ascertain the actual organ dose for each subject, it is necessary to multiply by the respective Conversion Factor (CF), as illustrated in Equation (1):

$$D_{kVp,width} = (D_{simulated})_{kVp,width} \cdot CF_{kVp,width}^{bowtie\ filter} \cdot \frac{(CTDI_{vol})_{kVp,width}^{clinical,per\ 100mAs}}{(CTDI_{vol})_{kVp,width}^{validated,per\ 100mAs}} \cdot \frac{mAs\ per\ rotation}{100} \quad (1)$$

$$D_{kVp,width}^{normalized} (mGy/CTDI_{vol}^{per\ 100mAs}) = \frac{(D_{simulated})_{kVp,width} \cdot CF_{kVp,width}^{bowtie\ filter}}{(CTDI_{vol})_{kVp,width}^{validated,per\ 100mAs}} \quad (2)$$

Where $D_{kVp,width}$ represents the actual organ dose for the subject in mGy. $(D_{simulated})_{kVp,width}$ signifies the organ dose simulated in Monte Carlo, with its unit being MeV/gram/photon. Both organ doses vary with the kVp and beam collimation width. $CF_{kVp,width}^{bowtie\ filter}$ is the experimentally validated conversion factor for GE LightSpeed Pro 16 MDCT in axial scanning¹⁵. This conversion factor varies with the kVp, beam collimation width, and bowtie filter, and is expressed in units of mGy·gram·photon/100mAs/MeV. $(CTDI_{vol})_{kVp,width}^{clinical,per\ 100mAs}$ refers to the CTDI_{vol} value displayed on the scanner during clinical CT examinations, normalized to 100 mAs per rotation. CTDI_{vol} is an effective parameter for comparison between different MDCT scanners. $(CTDI_{vol})_{kVp,width}^{validated,per\ 100mAs}$ is the value derived from previous research where the GE LightSpeed Pro 16 model was validated under similar

scanning conditions¹⁵. This value is also normalized to 100 mAs per rotation. *mAs per rotation* refers to the exposure expressed in mAs, which was set during clinical scanning. As shown in Equation (2), $D_{kVp,width}^{normalized} (mGy/CTDI_{vol}^{per\ mAs})$ represents the organ dose normalized by CTDI_{vol} per 100 mAs, for the subject in units of mGy/(CTDI_{vol} per 100 mAs). Value of CTDI_{vol} normalized organ dose eliminates the impact of CT machine model and scanning parameters.

To construct patient-specific phantoms of individual subjects, we employed the automatic organ segmentation software, DeepViewer (V1.2.0), based on the 3D ResU-Net architecture. The accuracy of segmentation by this software has been validated in our previous researches^{24–26}. Specifically, DeepViewer supports automatic segmentation of over 32 organs across various regions, including the head and neck, chest, abdomen, pelvis, and legs. When compared to segmentation results by experienced clinicians, for most organs throughout the body, the Dice Similarity Coefficient (DSC) achieved a value of 0.9. Major organs like the brain, both lungs, heart, liver, and kidneys even surpassed a DSC of 0.95.

To enable large-scale, patient-specific dose computations, we developed a preliminary CT dose computation and analysis software platform based on the dosimetry engine and implemented in MATLAB Version: 9.14.0 (R2023a). As illustrated in Figure 1, after the subject's CT images were automatically segmented and the corresponding patient-specific phantom was constructed, we performed a near real-time dose simulation on the phantom using a chest scan protocol similar to that used in clinical image acquisition. This allowed us to obtain patient-specific 3D dose distributions and organ doses.

Statistical analysis of health metrics and organ doses

Tables 1 and 2 present the chest CT scan parameter settings and statistics on age, gender, and body metrics for the 11,482 subjects. As shown in Table 1, the data cover scans from five different CT scanner models: GE Discovery CT750 HD, GE LightSpeed VCT, NMS NeuViz 128, GE Optima CT660, and GE Optima CT680 Series. Notably, for all the models, the kVp is uniformly set at 120, with a collimation width of 40 mm. Furthermore, all models utilize the body type of bowtie filter. As illustrated in Table 2, there are 7182 male subjects, with the average (\pm standard deviation) age (years), height (cm), weight (kg), BMI (kg/m²), average WED (cm) and scan range (cm) to be 49.8 (\pm 12.8), 170.6 (\pm 6.1), 73.9 (\pm 10.4), 25.3 (\pm 3.0), 26.2 (\pm 1.9), 36.0 (\pm 2.2), respectively. There are also 4300 female subjects, with the average age, height (cm), weight (kg), BMI (kg/m²), average WED (cm) and scan range (cm), to be 50.0 (\pm 13.0), 159.1 (\pm 5.7), 58.9 (\pm 8.4), 23.2 (\pm 3.1), 23.8 (\pm 2.0), 34.3 (\pm 1.9), respectively.

Table 1. Chest CT scanning parameter information extracted from the Digital Imaging and Communications in Medicine (DICOM) files of 11,482 subjects, including 5 CT scanner models and 13 scan protocols.

Scan protocol	CT model	Subjects	kVp (E)	Collimation width (mm) (NT)	Bowtie Filter	CTDI _{vol,100mAs} (mGy)	pitch	mAs per rotation
1	GE Discovery CT750 HD	234	120	40	Body	8.30	1.375	25.5
2	GE Discovery CT750 HD	229	120	40	Body	8.30	1.375	30.5
3	GE Discovery CT750 HD	922	120	40	Body	8.30	1.375	35.6
4	GE LightSpeed VCT	695	120	40	Body	9.51	1.375	25.5
5	GE LightSpeed	383	120	40	Body	9.51	1.375	30.5

	VCT							
6	GE LightSpeed VCT	789	120	40	Body	9.51	1.375	43.6
7	NMS NeuViz 128	984	120	40	Body	6.18	1.2	50
8	GE Optima CT660	5149	120	40	Body	8.71	1.375	30.5
9	GE Optima CT660	283	120	40	Body	8.71	0.984	56.9
10	GE Optima CT660	623	120	40	Body	8.71	0.984	97.5
11	GE Optima CT680 Series	456	120	40	Body	8.71	1.375	25.5
12	GE Optima CT680 Series	716	120	40	Body	8.71	1.375	40.7
13	Others	19	There were 13 different scan protocols for the 19 subjects					

Table 2. Statistics of average (\pm standard deviation) on age, gender, and body metrics for the 11,482 subjects. There are 7182 male subjects and 4300 female subjects.

Gender	Metric	Age	Height (cm)	Weight (kg)	BMI (kg/m ²)	Average WED (cm)	Scan range (cm)
male	Average	49.8 (\pm 12.8)	170.6 (\pm 6.1)	73.9 (\pm 10.4)	25.3 (\pm 3.0)	26.2 (\pm 1.9)	36.0 (\pm 2.2)
	Range	19 ~ 93	145.5 ~ 195	44.3 ~ 138.8	15.4 ~ 41.9	19.7 ~ 34.5	29.4 ~ 46.2
Female	Average	50.0 (\pm 13.0)	159.1 (\pm 5.7)	58.8 (\pm 8.4)	23.2 (\pm 3.1)	23.8 (\pm 2.0)	34.3 (\pm 1.9)
	Range	16 ~ 93	139 ~ 187	36.5 ~ 111.2	15.8 ~ 44.1	18.4 ~ 34.4	25.2 ~ 42.0

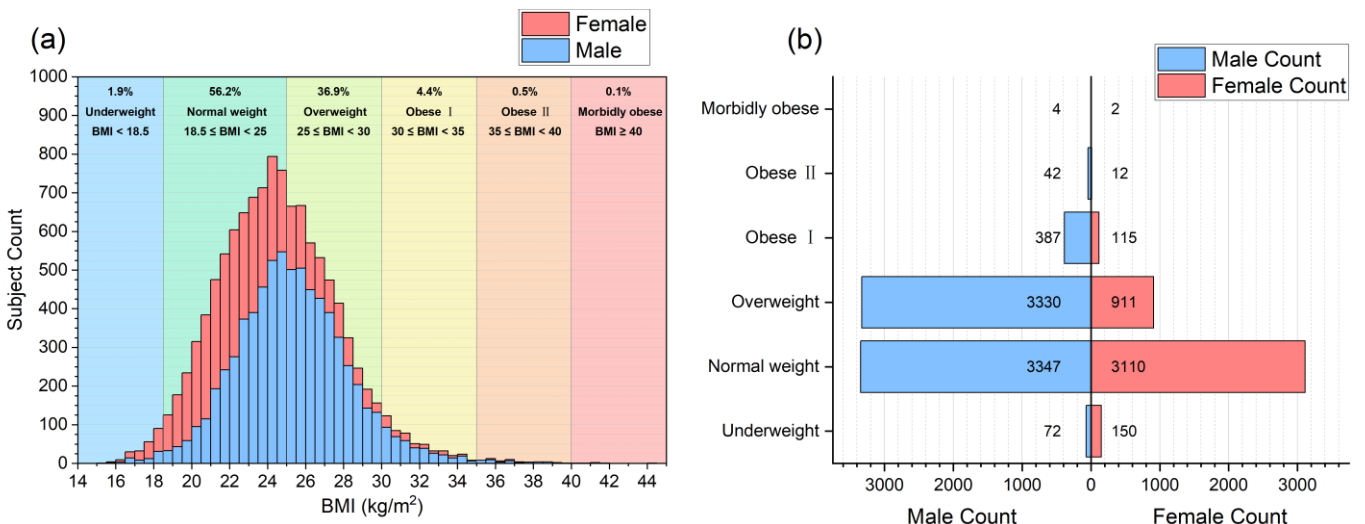


Figure 8. BMI classification statistics for male and female subjects. (a) Cumulative histogram of the number of subjects relative to their BMI, where red bars represent female subjects and blue bars represent male subjects.

(b) The number of male and female subjects in each of the six different BMI categories.

The BMI classification statistics for both male and female subjects included in this study are depicted in Figure 8. Among all subjects, 56.2% fall into the Normal weight category, while 36.9% are classified as Overweight. The other BMI categories account for 6.9% of the subjects. Notably, the BMI distribution varies between genders. Among males, the proportions of Normal weight and Overweight are similar. In contrast, in the female cohort, a significant 72% fall into the Normal weight category, compared to 21% in the Overweight category.

As illustrated in Figure 9, both the CT scanner model and scan parameter settings can impact the patient-specific organ dose. Because, as shown in Equation (1), $CTDI_{vol}$ is dependent on the CT scanner model, kVp, beam collimation width, and the type of bowtie filter. Additionally, $CTDI_{vol}$ is inversely proportional to the pitch factor of the helical scan, while the organ dose is directly proportional to exposure in mAs.

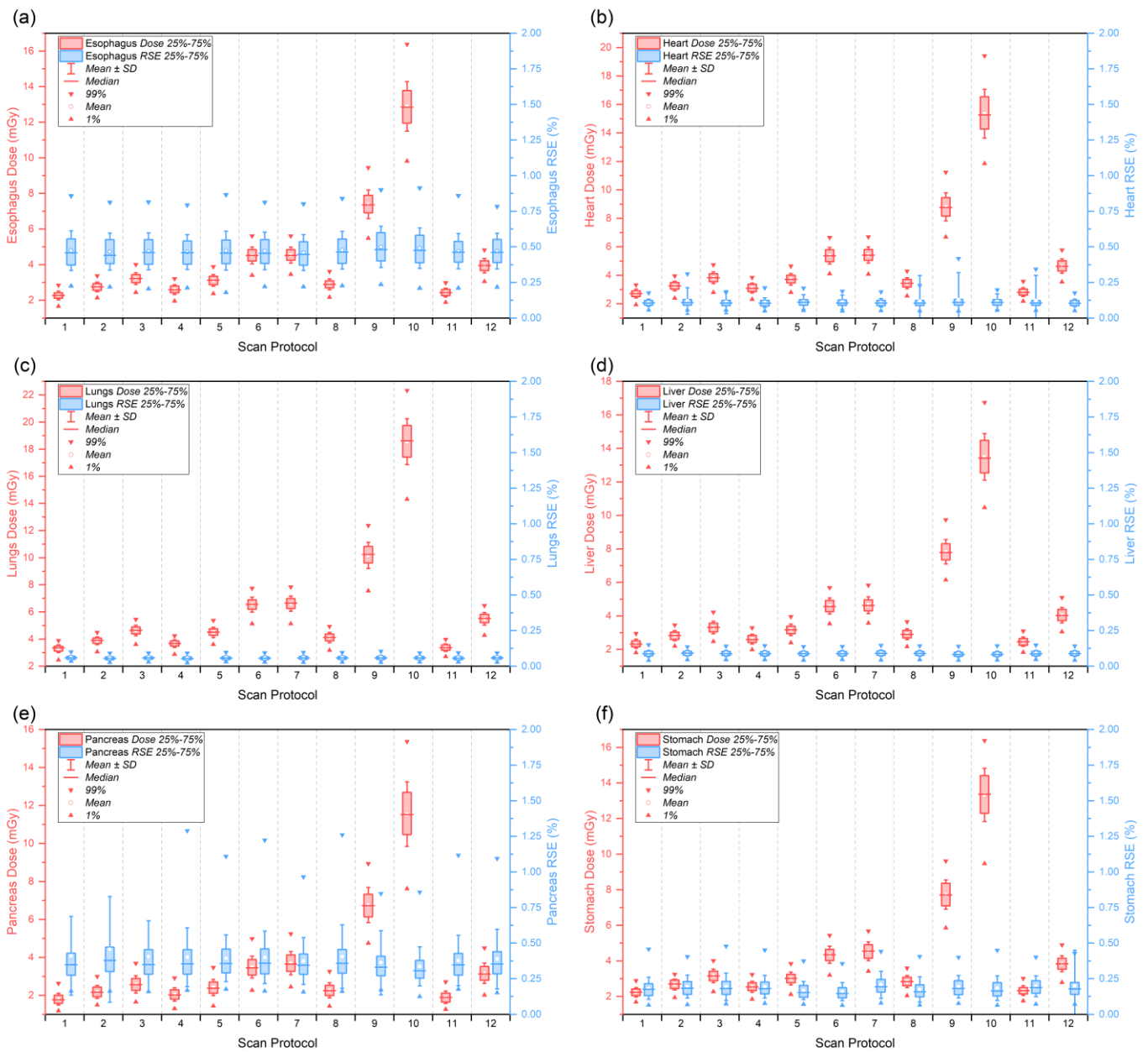


Figure 9. Box plots depicting dose results for the 6 organs and their corresponding statistical uncertainties (RSE) associated with scanning parameters. The red vertical axis shows the organ dose results for chest CT scan obtained using the proposed method, while the blue vertical axis displays the statistical uncertainties of the organ dose. The horizontal axis shows the first 12 scan protocols listed in the Table 1. (a) Results for esophagus. (b) Results for heart. (c) Results for lungs. (d) Results for liver. (e) Results for pancreas. (f) Results for stomach.

Additionally, as shown in Figure 10, we calculated the Pearson correlation coefficients to examine the relationship between CTDI_{vol} normalized organ doses and patient characteristics, such as age, height, weight, scan range, BMI, and average Water Equivalent Diameters (WED). These factors are unrelated to CT scan settings, but can potentially impact patient-specific organ dose values. The results indicate that height, weight, and average WED all demonstrate a moderate correlation with gender. There is a very strong correlation between weight, BMI, and average WED, with the correlation coefficient between weight and average WED reaching 0.91. The CTDI_{vol} normalized doses for thoracic organs reveal a weak correlation with both gender and height, while the normalized doses for abdominal organs shows a moderate correlation with both. The normalized doses for the lungs have a moderate correlation with average WED, whereas the normalized dose for other organs presents a strong correlation with average WED. The correlation coefficients between the normalized doses of different organs indicate that organs in closer anatomical proximity exhibit stronger dose correlations. For all the organs considered, the absolute value of correlation coefficients for normalized organ dose with BMI and average WED are greater than 0.5, peaking at 0.88 and 0.95, respectively, indicating a very strong linear relationship between them.

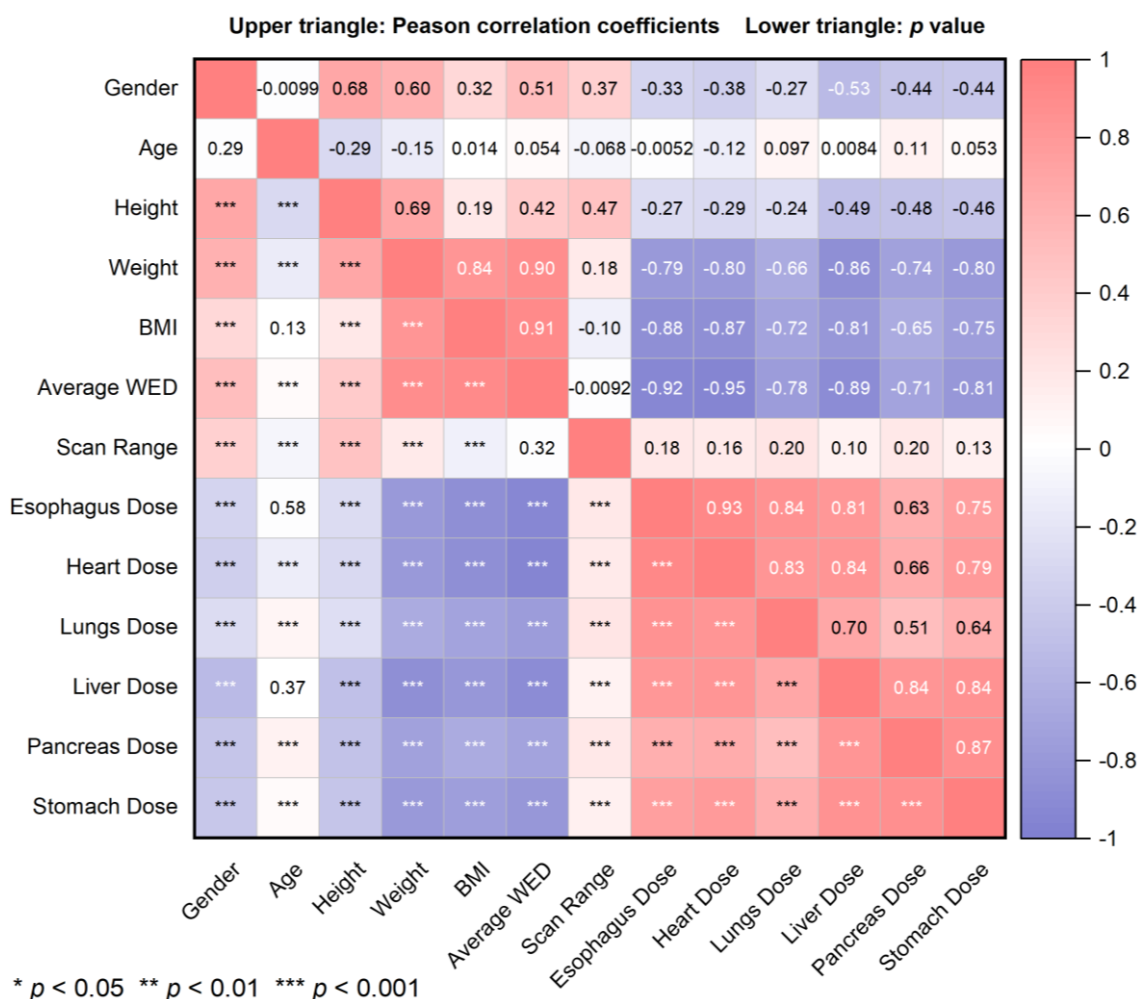


Figure 10. The Pearson correlation coefficients between the CTDI_{vol} normalized organ dose for chest CT scan and other factors for the subjects.

BMI categories

According to the BMI categories set by the World Health Organization globally²⁷, Table 3 summarizes the BMI data of the 11,482 subjects.

Table 3. Statistics of BMI categories for the 11,482 subjects.

Category	BMI Classification standard ²⁷ (kg/m ²)	Male subjects	Average (\pm standard deviation) BMI of the male (kg/m ²)	Female subjects	Average (\pm standard deviation) BMI of the female (kg/m ²)

Underweight	(0, 18.5)	72	17.6 (\pm 0.8)	150	17.7 (\pm 0.6)
Normal weight	[18.5, 25)	3347	23.0 (\pm 1.5)	3110	22.1 (\pm 1.7)
Overweight	[25, 30)	3330	26.9 (\pm 1.3)	911	26.8 (\pm 1.3)
Obese I	[30, 35)	387	31.6 (\pm 1.3)	115	31.6 (\pm 1.3)
Obese II	[35, 40)	42	36.7 (\pm 1.4)	12	36.7 (\pm 1.0)
Morbidly obese	[40, ∞)	4	41.3 (\pm 0.7)	2	42.4 (\pm 2.4)

Image pre-processing

Each slice of the DICOM CT images for all subjects maintained a pixel resolution of 512×512, with no resampling processes applied. The mean (\pm standard deviation) value of pixel size is 0.81 (\pm 0.04) mm. And the slice thickness for all subjects is 6 mm. The beds in each slice of the CT images for all subjects were removed.

Segmented organs

In this study, the automatic segmentation results of chest CT images for the 11,482 subjects included contours for 12 organs: body skin, spinal cord, esophagus, heart, lungs, trachea, duodenum, kidneys, liver, pancreas, stomach, and bowel. For brevity, our results analysis only considered the doses for six organs, which were fully encompassed in the CT images and were commonly focused on in radiation protection: esophagus, heart, lungs, liver, pancreas, and stomach.

Monte Carlo simulation

Based on the extracted parameters of the clinical scanning protocol (including kVp, exposure expressed in mAs, beam collimation width, bowtie filter type, and pitch), we used the integrated CT scanner model in ARCHER-CT to conduct axial scan simulations on the subjects' computational phantoms with the same scanning range as in the clinical setting. In the ARCHER-CT simulations, the validated GE LightSpeed Pro 16 scanner model was employed with parameter settings of 120kVp, a collimation width of 20 mm, and a body type of bowtie filter. The starting angle of the beam in helical scanning used clinically cannot be obtained from the DICOM protocol, while its variation might cause significant discrepancies in the simulated dose for small organs^{23,32}. Moreover, the radiation dose in helical scanning is inversely related to the pitch when other scanning parameters remain constant. And if helical scanning (pitch \neq 1) is converted into helical scanning with a pitch of 1, its radiation dose is approximately the same as that generated by continuous axial scanning under the same scanning parameters^{33,34}. Therefore, in this study, we used continuous axial scanning simulations to replace helical scanning used clinically. Furthermore, both actual clinical scans and MC simulations did not use TCM. However, if the tube current values of every slice used in TCM can be obtained, it can be easily imported into ARCHER-CT to change the proportion of particle histories at each projection angle in MC simulations.

In the ARCHER-CT simulations, identical scanning parameters were applied to both the ICRP phantoms and the subjects. For the ICRP phantoms, the total number of photon histories used for MC simulation was 10^{10} to maintain the statistical uncertainty (Relative Standard Error, RSE) of all organ doses within 0.1%. The scan range chosen for the phantoms closely mirrored the chest range typically employed in clinical settings. For each subject, the total number of photon histories used for MC simulation was 10^8 to maintain the statistical uncertainty of most organ doses within 1%, with only the uncertainty of organ doses that are deep and small in volume possibly exceeding 1%.

Hardware configuration

In this study, both DeepViewer and ARCHER-CT were executed on a commercially available consumer-grade PC, equipped with specific hardware configurations: Intel® Core™ i7-12700 CPU, 64 GB DDR4 memory, and a single NVIDIA GeForce RTX™ 3080 10GB GPU.

Statistical analysis tools

In this study, most numeric results are represented as mean \pm standard deviation. This representation provides a concise view of the central tendency and variability within our dataset. Statistical significance was assessed using a Pearson correlation test. The p values were obtained and represented with asterisk, with * indicating $p < 0.05$, ** indicating $p < 0.01$, and *** indicating $p < 0.001$. The Pearson correlation coefficient, ranging from -1 to 1, measures the strength and direction of the linear relationship between two variables. A coefficient of -1 indicates a perfect negative correlation, 1 signifies a perfect positive correlation, and 0 indicates no correlation. Statistical analysis of the results was conducted using OriginPro 2021b.

Data availability

The 11,482 cases of subjects' data were obtained from the Health Center of the First Affiliated Hospital of USTC (Hefei, China), where partial data (i.e., 50 anonymous cases) are released together with the code, with the permission obtained from respective health center. The full dataset is protected because of privacy issues and regulation policies in health center.

Code availability

Excel files of results and MATLAB scripts used in data processing will be found in the GitHub repository.

References

1. United Nations: Scientific Committee on the Effects of Atomic Radiation. *UNSCEAR 2020/2021 Report Volume I, Scientific Annex A: 'Medical exposure to ionizing radiation'*. (United Nations, 2022).
2. National Council on Radiation Protection and Measurements. *Medical radiation exposure of patients in the United States: recommendations of the National Council on Radiation Protection and Measurements*. (NCRP, 2019).
3. Yao, J., Gao, L., Qian, A. & Wang, B. Survey on frequency of medical X-ray diagnosis in Shanghai. *Chin. J. Radiol. Med. Prot.* **39**, 370–375 (2019).
4. Bosch de Basea Gomez, M. *et al.* Risk of hematological malignancies from CT radiation exposure in children, adolescents and young adults. *Nat. Med.* **29**, 3111–3119 (2023).
5. National Research Council. *Health Risks from Exposure to Low Levels of Ionizing Radiation: BEIR VII Phase 2*. (The National Academies Press, 2006).
6. Rogers, D. W. O. Fifty years of Monte Carlo simulations for medical physics. *Phys. Med. Biol.* **51**, R287–R301 (2006).
7. Huda, W. & Mettler, F. A. Volume CT Dose Index and Dose-Length Product Displayed during CT: What Good Are They? *Radiology* **258**, 236–242 (2011).

8. Turner, A. C. *et al.* The feasibility of a scanner-independent technique to estimate organ dose from MDCT scans: Using to account for differences between scanners. *Med. Phys.* **37**, 1816–1825 (2010).
9. Boone, J. *et al.* *AAPM Report No. 204: Size-Specific Dose Estimates (SSDE) in Pediatric and Adult Body CT Examinations.* 1–30 (2011).
10. McCollough, C. H. *et al.* Achieving Routine Submillisievert CT Scanning: Report from the Summit on Management of Radiation Dose in CT. *Radiology* **264**, 567–580 (2012).
11. Tian, X. *et al.* Dose coefficients in pediatric and adult abdominopelvic CT based on 100 patient models. *Phys. Med. Biol.* **58**, 8755–8768 (2013).
12. Xu, X. G. An exponential growth of computational phantom research in radiation protection, imaging, and radiotherapy: a review of the fifty-year history. *Phys. Med. Biol.* **59**, R233–R302 (2014).
13. Xu, X. G. *Computational Phantoms for Radiological Physics and Biomedical Engineering: the History and Future.* (Science Press, 2020).
14. Ban, N. *et al.* Development of a web-based CT dose calculator: WAZA-ARI. *Radiat. Prot. Dosimetry* **147**, 333–337 (2011).
15. Ding, A. *et al.* VirtualDose: a software for reporting organ doses from CT for adult and pediatric patients. *Phys. Med. Biol.* **60**, 5601–5625 (2015).
16. Lee, C., Kim, K. P., Bolch, W. E., Moroz, B. E. & Folio, L. NCICT: a computational solution to estimate organ doses for pediatric and adult patients undergoing CT scans. *J. Radiol. Prot. Off. J. Soc. Radiol. Prot.* **35**, 891–909 (2015).
17. Ramos, J. O. *et al.* MIRDct: a computed tomography dosimetry software - initial development and overview. *J. Nucl. Med.* **63**, 2654 (2022).
18. International Commission on Radiological Protection. Adult Reference Computational Phantoms. *ICRP Publ. 110 Ann* **39**, 1–165 (2009).
19. Thierry-Chef, I. *et al.* Dose Estimation for the European Epidemiological Study on Pediatric Computed Tomography (EPI-CT). *Radiat. Res.* **196**, 74–99 (2021).

20. Shi, F. *et al.* Deep learning empowered volume delineation of whole-body organs-at-risk for accelerated radiotherapy. *Nat. Commun.* **13**, 6566 (2022).
21. Xu, X. G. *et al.* ARCHER, a new Monte Carlo software tool for emerging heterogeneous computing environments. *Ann. Nucl. Energy* **82**, 2–9 (2015).
22. Adam, D. P., Liu, T., Caracappa, P. F., Bednarz, B. P. & Xu, X. G. New capabilities of the Monte Carlo dose engine ARCHER-RT: Clinical validation of the Varian TrueBeam machine for VMAT external beam radiotherapy. *Med. Phys.* **47**, 2537–2549 (2020).
23. Sharma, S. *et al.* A real-time Monte Carlo tool for individualized dose estimations in clinical CT. *Phys. Med. Biol.* **64**, 215020–215031 (2019).
24. Peng, Z. *et al.* A method of rapid quantification of patient-specific organ doses for CT using deep-learning-based multi-organ segmentation and GPU-accelerated Monte Carlo dose computing. *Med. Phys.* **47**, 2526–2536 (2020).
25. Wang, Z. *et al.* Evaluation of deep learning-based auto-segmentation algorithms for delineating clinical target volume and organs at risk involving data for 125 cervical cancer patients. *J. Appl. Clin. Med. Phys.* **21**, 272–279 (2020).
26. Chang, Y. *et al.* Clinical application and improvement of a CNN-based autosegmentation model for clinical target volumes in cervical cancer radiotherapy. *J. Appl. Clin. Med. Phys.* **22**, 115–125 (2021).
27. WHO Consultation on Obesity (1999: Geneva, Switzerland) & World Health Organization. *Obesity: preventing and managing the global epidemic: report of a WHO consultation*. 1–252 (2000).
28. McCollough, C. *et al.* AAPM Report No. 220: Use of Water Equivalent Diameter for Calculating Patient Size and Size-Specific Dose Estimates (SSDE) in CT. 1–23 (2014).
29. Martin, C. J., Harrison, J. D. & Rehani, M. M. Effective dose from radiation exposure in medicine: Past, present, and future. *Phys. Med.* **79**, 87–92 (2020).
30. Gu, J., Bednarz, B., Caracappa, P. F. & Xu, X. G. The development, validation and application of a multi-detector CT (MDCT) scanner model for assessing organ doses to the pregnant patient and the fetus using Monte Carlo

simulations. *Phys. Med. Biol.* **54**, 2699–2717 (2009).

31. Pi, Y., Liu, T. & Xu, X. G. DEVELOPMENT OF A SET OF MESH-BASED AND AGE-DEPENDENT CHINESE PHANTOMS AND APPLICATION FOR CT DOSE CALCULATIONS. *Radiat. Prot. Dosimetry* **179**, 370–382 (2018).
32. Zhang, D. *et al.* Reducing radiation dose to selected organs by selecting the tube start angle in MDCT helical scans: A Monte Carlo based study. *Med. Phys.* **36**, 5654–5664 (2009).
33. McNitt-Gray, M. F., Cagnon, C. H., Solberg, T. D. & Chetty, I. Radiation dose in Spiral CT: The relative effects of collimation and pitch. *Med. Phys.* **26**, 409–414 (1999).
34. Pan, Y. *et al.* Development of 1-year-old computational phantom and calculation of organ doses during CT scans using Monte Carlo simulation. *Phys. Med. Biol.* **59**, 5243–5260 (2014).

Acknowledgements

The authors are grateful to Yingming Zhao of Department of Radiology at the First Affiliated Hospital of USTC, for discussing the analysis method of subjects' image data. The study is supported by the following funding: Anhui Province Key Research and Development Plan (2023s07020020), National Natural Science Foundation of China (12275372), USTC Fund for the Development of Medical Physics and Biomedical Engineering Interdisciplinary Subjects (YD2140000601), USTC Fund for New Medicine - Innovation Team Project (YD2140002002).

Author contributions

Study conception and design: X.G.X., Z.Y., Z.C. and X.P.; Data collection: B.Y., H.Z. and Y.L.; Data analysis: Z.Y.; Interpretation of results: Z.Y. and X.G.X.; Manuscript preparation: Z.Y., L.T., R.W. and X.G.X. All authors reviewed the results and approved the final version of the manuscript.

Competing interests

X.G.X., X.P. and Y.L. are employees of Anhui Wisdom Technology Co., Ltd., Hefei, China (<http://wisdom-tech.com.cn/>). The company has no role in designing and performing the surveillance and analyzing and interpreting the data. All other authors report no conflicts of interest relevant to this article.